Available online at www.sciencedirect.com

ScienceDirect

IFAC Papers Online CONFERENCE PAPER ARCHIVE

IFAC-PapersOnLine 49-23 (2016) 251–257

A Tension-based Position Estimation Solution of a Moored Structure and its Uncertain Anchor Positions ⋆

Zhengru Ren *,** **Roger Skjetne** *,**

* *Centre for Research-based Innovation on Marine Operations (SFI MOVE), Department of Marine Technology, Norwegian University of Science and Technology, NTNU, NO-7491 Trondheim, Norway, (e-mail: zhengru.ren@ntnu.no, roger.skjetne@ntnu.no)*

** *Centre for Autonomous Marine Operations and Systems (AMOS), Department of Marine Technology, Norwegian University of Science and Technology, NTNU, NO-7491 Trondheim, Norway*

Abstract: Thruster-assisted position mooring (TAPM) is an attractive stationkeeping solution for long-term operation. Due to the complex environmental loads and system structure, increasing attention has been paid to improve the redundancy and reliability. This paper summaries the key research results when introducing the simultaneous localization and mapping algorithm to moored structures, which can provide an additional position reference system with uncertain anchor positions. It is especially cost-efficient for some applications alleviating the need for special sensors, such as, hydroacoustic sensors. The line-of-sight range mapping from tension measurements is discussed. Fairleads, the turret dynamics, and loading effects are considered to provide a more realistic and robust solution. A sensor network scheme and a state-space model are proposed, and an extended Kalman filter (EKF) is employed to estimate the uncertain anchor position.

Keywords: Thruster-assisted position mooring; map aided localization; SLAM

1. INTRODUCTION

Since oil exploration moves towards deeper waters, thruster-assisted position mooring (TAPM) has become an attractive stationkeeping solution for long-term operation (Skjetne et al., 2014). With the increasing attention to safety and new technological innovations, newly built TAPMs tend to be equipped with tension cells, which gives availability of tension measurements. A winch load monitoring system can enhance the systematic autonomy, as well as detect fatigue and line breakage (May et al., 2008). Aamo and Fossen (1999) theoretically addresses a robust dynamic mooring tension control scheme. The experimental verifications are conducted in Nguyen et al. (2011) and Ji et al. (2015). Furthermore, tension measurements may potentially be used to estimate the current profile (Ren and Skjetne, 2016).

It has been reported by the main class societies that one anchor is lost per 100 ships each year (Gard News, 2011). The risk of losing anchors and chains is tremendous when considering the service life in more than 20 years. The broken chains and anchors are considered as wrecks. According to the IMO convention, shipowners has the financial responsibility to the wreck removal (Ratcovich, 2008). Therefore, techniques which can quickly locate and remove the lost anchors are valuable.

Collaborative position location is a localization technique. Nodes in a sensor network can determine their locations collaboratively. It can be classified into deterministic and probabilistic methods. Approaches based on the maximum likelihood, such as the second-order cone programing (SOCP) and semi-definite programming (SDP), are widely-applied deterministic optimization-based approaches (Naddafzadeh-Shirazi et al., 2014; Tseng, 2007). Ren et al. (2015) applies a tension-based scheme to locate the position of the moored vessel with known anchor positions. The anchors are then regarded as landmarks. However, the application of the algorithm is limited by the precise knowledge of the positions of the anchors. The above-mentioned methods are not robust enough, since a moored structure can only move in a limited region much smaller than the footprints of the mooring lines. Hence, the anchor positions may not be distinguishable. Simultaneous localization and mapping (SLAM) is a relatively new technique applied in robotics to locate the robot with uncertain landmarks and no access to position reference (posref) through a joint estimation of pose and landmarks (Gustafsson, 2010). Normally, extended Kalman filter (EKF), particle filter, and FastSLAM are the most popular approaches (Durrant-Whyte and Bailey, 2006).

This paper adapts the map aided localization technique to the TAPM system. The key application is to locate the vessel with tension measurements. In addition, a simplified model is used to track the uncertain anchor positions for any vessels equipped with tension cells. With precise localization and short operation period, the costs to remove the lost anchors will be reduced.

1.1 Terminology

In this paper, an *anchor* and an *anchor node* are two different terms with unlike meanings. We define them as follows:

Definition 1. (Anchor). An anchor is a heavy device attached to a cable or chain which is used to prevent the craft from drifting due to environmental loads (Oxford Advanced Learner's Dictionary, n.d.).

Definition 2. (Anchor node). An anchor node is a node in a sensor network whose position is expected to have been known (Zekavat and Buehrer, 2011). We can also call it a landmark.

⋆ This work was supported by the Research Council of Norway (RCN) through the Centre for Research-based Innovation on Marine Operations (RCN-project 237929), and partly by the Centre of Excellence AMOS (RCN-project 223254).

10.1016/j.ifacol.2016.10.351

2. SYSTEM MODELING

A surface vessel is spreadly moored by M anchor lines and equipped with thruster assist. Each mooring line is connected to the turret through the corresponding fairlead (see Fig. 1(a)). The vessel motion is assumed to be represented in 3DOF by surge, sway, and yaw. The environmental loads are wind, waves, and currents. The Earth-fixed north-east-down (NED) and body-fixed coordinate systems, $\{E\}$ and $\{B\}$, are employed in this paper. The origin of the NED frame is located at the field zero point (FZP) which is the equilibrium position where the vessel comes to rest without any environmental and thruster loads. The turret can rotate about a vertical axis at the center of turret (COT) for simplification. The motion can be superposed by the low-frequency (LF) model and the wave-frequency (WF) model (Fossen, 2011).

2.1 Vessel model

In what follows, the vessel model described in Fossen (2011) is given by

$$\dot{\boldsymbol{\eta}} = \boldsymbol{R}(\psi)\boldsymbol{\nu}, \tag{1a}$$
$$\dot{\boldsymbol{b}} = -\boldsymbol{T}_b^{-1}\boldsymbol{b} + \boldsymbol{E}_b\boldsymbol{w}_b, \tag{1b}$$
$$\boldsymbol{M}\dot{\boldsymbol{\nu}} = -\boldsymbol{D}\boldsymbol{\nu} + \boldsymbol{R}(\psi)^\top\boldsymbol{b} + \boldsymbol{\tau}_m + \boldsymbol{\tau}_c \tag{1c}$$
$$\dot{\boldsymbol{\xi}} = \boldsymbol{A}_w\boldsymbol{\xi} + \boldsymbol{E}_w\boldsymbol{w}_w, \tag{1d}$$
$$\boldsymbol{\eta}_w = \boldsymbol{C}_w\boldsymbol{\xi}, \tag{1e}$$

where $\boldsymbol{\eta} = [x\ y\ \psi]^\top$ consists of LF position and heading orientation of the vessel relative to the NED frame, $\boldsymbol{\nu} = [u\ v\ r]^\top$ represents the vector of transverse and angular velocities decomposed in the body-fixed reference, $\boldsymbol{R}(\psi) \in \mathbb{R}^{3\times3}$ denotes the rotation matrix between the body-fixed frame and the NED frame (see Fig. 1(a)), $\boldsymbol{E}_b \in \mathbb{R}^{3\times3}$ is a diagonal scaling matrix, $\boldsymbol{M} \in \mathbb{R}^{3\times3}$ is the generalized system inertia matrix including zero frequency added mass components, $\boldsymbol{D} \in \mathbb{R}^{3\times3}$ denotes the linear damping matrix, $\boldsymbol{b} \in \mathbb{R}^3$ is a slowly varying bias vector in the NED frame, $\boldsymbol{\tau}_c \in \mathbb{R}^3$ represents the thruster-induced loads, and $\boldsymbol{\tau}_m \in \mathbb{R}^3$ is the mooring loads. $\boldsymbol{\xi} = [\xi_1, \xi_2, \xi_3, \xi_4, \xi_5, \xi_6]^\top \in \mathbb{R}^6$, $\boldsymbol{\eta}_w \in \mathbb{R}^3$ is the WF motion vector, $\boldsymbol{w}_w \in \mathbb{R}^3$ is a zero-mean Gaussian white noise vector, $\boldsymbol{A}_w \in \mathbb{R}^{6\times6}$, $\boldsymbol{C}_w \in \mathbb{R}^{3\times6}$, and $\boldsymbol{E}_w \in \mathbb{R}^{6\times3}$ are the system matrix, measurement matrix, and diagonal scaling matrix of the linear filter. See Fossen (2011) for details.

2.2 Mooring forces

The mooring system is simulated by a FEM model. A horizontal-plane spread mooring model is formulated as

$$\boldsymbol{\tau}_m = -\boldsymbol{R}(\psi)^\top\boldsymbol{g}_{mo} - \boldsymbol{D}_{mo}\boldsymbol{\nu}, \tag{2}$$

where it is assumed that the mooring system is symmetrically arranged. The Earth-fixed restoring force and moment vector acting at the moored vessel is given by

$$\boldsymbol{g}_{mo} = \begin{bmatrix} \boldsymbol{g}^t_{mo,1:2} \\ D^t_z\dot{\tilde{\psi}}_t \end{bmatrix}, \tag{3}$$

where $\boldsymbol{g}^t_{mo}$ is the restoring force and moment vector acting at the turret, the subscript $1:2$ means the first and second elements in the vector, ψ_t is the angle of the turret comparing with the reference, $\tilde{\psi}_t = \psi_t - \psi$ is the relative angle between the turret and the heading of the moored vessel. The dynamic model of $\tilde{\psi}_t$ is given by

$$I^t_z\ddot{\tilde{\psi}}_t = -g^t_{mo,3} - D^t_z\dot{\tilde{\psi}}_t, \tag{4}$$

where I^t_z is the mass inertia of moment of the turret and D^t_z is the damping between the vessel and the turret. The restoring forces

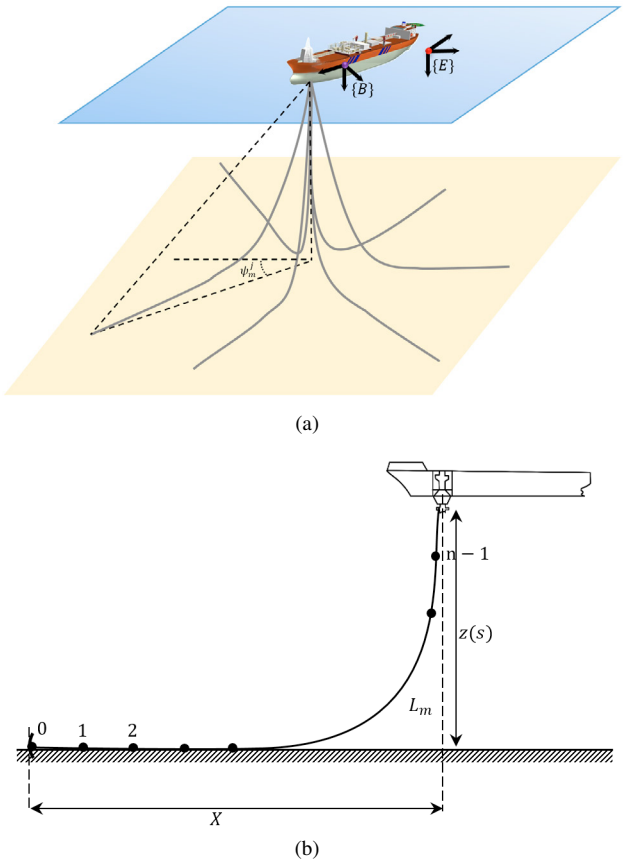

Fig. 1. (a) Reference frames, (b) finite element method (FEM) model of a mooring line.

and moment vector $\boldsymbol{g}^t_{mo}(\boldsymbol{\eta}) \in \mathbb{R}^3$, which the mooring lines exert on the turret, is given by

$$\boldsymbol{g}^t_{mo} = \sum_{i=1}^{M}\begin{bmatrix} \boldsymbol{f}^i_{mo,1:2} \\ \boldsymbol{f}^i_{mo,1:2} \times (\boldsymbol{p}^i_f - \boldsymbol{p}_{COT}) \end{bmatrix}, \tag{5}$$

where $\boldsymbol{f}_{mo} \in \mathbb{R}^3$ is the generalized force at the end of the cable, respectively, in x, y, and z direction. The horizontal position of a fairlead $\boldsymbol{p}^i_f \in \mathbb{R}^2$ are given by

$$\boldsymbol{p}^i_f = \boldsymbol{p}_{COT} + \begin{bmatrix} r_t\cos(\gamma^i_f) \\ r_t\sin(\gamma^i_f) \end{bmatrix}, \quad i = 1, \cdots, M, \tag{6}$$

where $\boldsymbol{p}_{COT} \in \mathbb{R}^2$ is the horizontal position of the COT. For simplification, we consider a situation that the COT overlaps with the center of gravity (COG) of the vessel in this paper, i.e., $\boldsymbol{p}_{COT} = [x, y]^\top$. The horizontal position of the i^{th} fairlead is represented by $\boldsymbol{p}^i_f \in \mathbb{R}^2$, r_t is the radius of the circle where the fairleads locate, and γ^i_f is the angle of the i^{th} fairlead compared to the reference angle.

The FEM model is developed in Aamo and Fossen (2001). With the proof of the existence and uniqueness of the solution, it can be used to simulate the mooring line in the time domain. The unstretched length of the i^{th} cable is L^i. Each of the mooring line is uniformly divided into n segments of length $l^i = L^i/n$, and the weight of all segments concentrate at all the $n+1$ nodes. From the anchor to the fairlead, the nodes are enumerated from 0 to n. The position vector of the k^{th} node along the i^{th} cable in the Earth-fixed coordinate is denoted by $\boldsymbol{r}^i_k \in \mathbb{R}^3$. The positions of the bottom and top end nodes are the anchor and the fairlead, i.e., $\boldsymbol{r}^i_{0,1:2} = \boldsymbol{p}^i_a$ and $\boldsymbol{r}^i_{n,1:2} = \boldsymbol{p}^i_f$. A node is only influenced by its

nearest neighboring nodes. The Galerkin method, which refers to a group of ordinary differential equations, is applied to all nodes in the time domain, given by

$$\left[\left(\rho_0 l^i + \frac{C_1^i}{2}\left(\varepsilon_k^i + \varepsilon_{k+1}^j\right)\right)\boldsymbol{I}_{3\times3} - \frac{C_1^i}{2}\left(\frac{\boldsymbol{l}_k^i \boldsymbol{l}_k^{i\top}}{\varepsilon_k^j} + \frac{\boldsymbol{l}_{k+1}^i \boldsymbol{l}_{k+1}^{i\top}}{\varepsilon_{k+1}^i}\right)\right]\ddot{\boldsymbol{r}}_k^i = \boldsymbol{f}_{k_{(r)}}^i + \boldsymbol{f}_{k_{(hg)}}^i + \boldsymbol{f}_{k_{(dt)}}^i + \boldsymbol{f}_{k_{(dn)}}^i,\ i = 1,\cdots,M,\ k = 1,\cdots,n-1, \tag{7}$$

where

$$\boldsymbol{l}_k^i = \boldsymbol{r}_k^i - \boldsymbol{r}_{k-1}^i, \quad e_k^i = \frac{|\boldsymbol{l}_k^i|}{l^i} - 1, \quad \varepsilon_k^i = |\boldsymbol{l}_k^i|, \quad \boldsymbol{P}_k^i = \frac{\boldsymbol{l}_k^i \boldsymbol{l}_k^{i\top}}{\varepsilon_k^{i\,2}},$$

$$C_1^i = C_{MN}^i \frac{\pi d_i^2}{4}\rho_w, \quad C_2^i = \frac{1}{2}C_{DT}^i d_i \rho_w, \quad C_3^i = \frac{1}{2}C_{DN}^i d_i \rho_w,$$

$$\boldsymbol{f}_{k_{(r)}}^i = EA_0\left[\frac{e_{k+1}^i}{\varepsilon_{k+1}^i}\boldsymbol{l}_{k+1}^i - \frac{e_k^i}{\varepsilon_k^i}\boldsymbol{l}_k^i\right],$$

$$\boldsymbol{f}_{k_{(hg)}}^i = l^i \rho_0^i \frac{\rho_c^i - \rho_w}{\rho_c^i}[0\ 0\ g]^\top,$$

$$\boldsymbol{f}_{k_{(dt)}}^i = -\frac{C_2^i}{2}\left[\left|\dot{\tilde{\boldsymbol{r}}}_k^i \cdot \boldsymbol{l}_k^i\right|\boldsymbol{P}_k^i + \left|\dot{\tilde{\boldsymbol{r}}}_k^i \cdot \boldsymbol{l}_{k+1}^i\right|\boldsymbol{P}_{k+1}^i\right]\dot{\tilde{\boldsymbol{r}}}_k^i,$$

$$\boldsymbol{f}_{k_{(dn)}}^i = -\frac{C_3^i}{2}[\varepsilon_k^i\left|\left(\boldsymbol{I}_{3\times3} - \boldsymbol{P}_k^i\right)\dot{\tilde{\boldsymbol{r}}}_k^i\right|\left(\boldsymbol{I}_{3\times3} - \boldsymbol{P}_k^i\right) + \varepsilon_{k+1}^i\left|\left(\boldsymbol{I}_{3\times3} - \boldsymbol{P}_{k+1}^i\right)\dot{\tilde{\boldsymbol{r}}}_k^i\right|\left(\boldsymbol{I}_{3\times3} - \boldsymbol{P}_{k+1}^i\right)]\dot{\tilde{\boldsymbol{r}}}_k^i,$$

the superscript and subscript i identifies the i^{th} cable, $\rho_0 = \frac{\pi d_i^2}{4}(\rho_c^i - \rho_w)g$ is the mass per unit length of the unstretched cable, ρ_c and ρ_w stand for the cable density and the ambient water density, d denotes the cable diameter, g represents the gravity acceleration, C_{MN} refers to the added mass coefficient, C_{DT} and C_{DN} are the tangential and normal drag coefficients of the cable, e is the strain, E is the Young's modulus of elasticity, $A_0^i = \frac{\pi}{4}d_i^2$ stands for the cross-section area of the unstretched cable, $\boldsymbol{f}_{k_{(hg)}}$, $\boldsymbol{f}_{k_{(r)}}$, and $\boldsymbol{f}_{k_{(dt)}}$ and $\boldsymbol{f}_{k_{(dn)}}$ are the buoyancy force, the reaction force, and the tangential and normal hydrodynamic drag per unit length of the unstretched cable, respectively. The top ends, i.e., $k = n$, are determined by the motion of the fairleads. The relative velocity in the Earth-fixed reference frame at the depth of the k^{th} node is $\dot{\tilde{\boldsymbol{r}}}_k^i = \dot{\boldsymbol{r}}_k^j - \boldsymbol{v}_c^k$, where $\boldsymbol{v}_c^k$ are the current velocity at the depth of the k^{th} node. The FEM model is initialized by the catenary equations. The generalized mooring force at the fairlead depends on the position of the nodes labeled with $n-1$ and n, such that $\boldsymbol{f}_{mo}^i = \frac{EA_0 e_n^i}{\varepsilon_n^i}\boldsymbol{l}_n^i$. See Aamo (1999) for more details.

3. RANGE MEASUREMENT

3.1 Mapping from tension to range

Now, efforts are paid on the range measurements from the tension measurements. The tension of a specific catenary mooring line exposed to gravity acts as a restoring force to the moored vessel. Based on the iteration results of catenary equations, there exists a mapping between the tension and range in the undisturbed environment. Therefore, we have the following assumption.

Assumption 1. (Tension-range mapping). When the anchor is fixed, there exists a map between the tension at its upper end and the horizontal projected distance between the i^{th} anchor and the upper end, such that

$$T_i^0 = f_i(X_i^0) + \Delta T_{i,c} + \Delta T_{i,v} + \Delta T_{i,s},\ i = 1,\cdots,M, \tag{8}$$

where T_i^0 is the noiseless axial tension at the top end of the i^{th} mooring line, X_i^0 is the distance between the i^{th} anchor and its fairlead, $f_i : D_{X_i} \mapsto \mathbb{R}$ is a locally Lipschitz map from the feasible region $D_{X_i} \subset \mathbb{R}$ into the axial tension when $z = 0$, $\Delta T_{i,c}$, $\Delta T_{i,v}$ and $\Delta T_{i,s}$ are the tension variances due to the current load, the wave-induced motion, and the seafloor topographical difference from the proposed catenary equation.

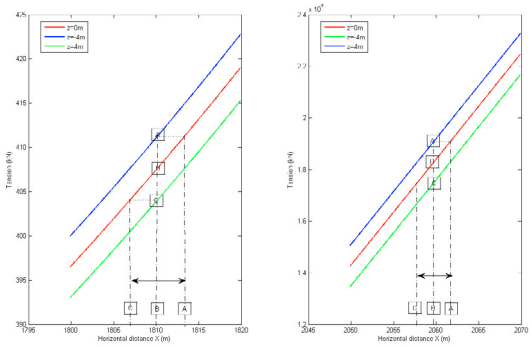

Fig. 2. The influence of the wave-induced heave motion at different part.

First we disregard $\Delta T_{i,c}$, $\Delta T_{i,v}$ and $\Delta T_{i,s}$, and define

$$T_{ij}^0 = f_i(X_{ij}^0) \text{ and } T_i^0 = f_i(X_i^0), \tag{9}$$

where X_{ij}^0 is the horizontal distance between the i^{th} anchor and the fairlead of a j^{th} "virtual" vessel's turret, which will be illustrated later. Based on the iteration results of the quasi-static analysis, f_i is a continuous strictly monotonic function. Therefore, f_i is bijective with an inverse function f_i^{-1}. In other words, we can estimate the horizontal projected distance between the anchor and fairlead through a perfect tension measurement, such that $X_i^0 = f_i^{-1}(T_i^0)$.

3.2 Noise in the range measurements

The actual situation is more complex. There are disturbances and noise in the range measurements (9). The disturbances are due to an exteroceptive bias caused by the tension cells, as well as a proprioceptive bias caused by current, seafloor topography, loading, and model uncertainty. The influence of biases will be discussed in further publications. In this paper, we briefly discuss the effect of noise in the range measurement.

When the vessel's position in the z direction changes, the axial tensions in the cables are influenced. The mechanics of the effects from heave motion is demonstrated in Fig. 2. The curves are the iteration results for a specific mooring line with different projected distance on the seafloor and heave based on the catenary equations. Assume the real range is at the point B. Relying on the mapping relation at $z = 0\ m$, shown as the red line, the inverse mapping gives a distance as the point A when the vessel heaves at $z = -4\ m$; the distance appears to stay at the point C when $z = 4\ m$. We notice the influence depends on the slope of curve and the magnitude of the heave motion.

We also notice the slope of the tension variance due to heave motion is almost a constant near the equilibria. Therefore, the partial derivative of the tension with respective to heave motion is almost linear, such that $\frac{\partial T_i^0}{\partial z} \approx$ constant. Since the mean heave motion is zero, we assume the dynamic tension from WF motion is an independent zero-mean Gaussian white noise process.

When a mooring line is subjected to current loads, we can find the top tension is influenced. However,current has a small impact on the top tension; and hence the current-induced tension

variance is disregarded. The noisy tension measurement after loading-correction is given by

$$T_{ij} = T_{ij}^0 + v_{tij} + \frac{k_{Ti}\Delta W_j}{A_w \rho_w g} \text{ and } T_i = T_i^0 + v_{ti} + \frac{k_{Ti}\Delta W}{A_w \rho_w g}, \quad (10)$$

where $v_{ti} \sim N(0, \sigma_{Tn_i}^2)$ and $v_{tij} \sim N(0, \sigma_{Tn_i}^2)$ are the zero-mean Gaussian white noise of the i^{th} tension cell, $k_{Ti} = \frac{\partial T_i^0}{\partial z}$ is a correction factor for the influence of the load variance, ΔW is the changed loading, and A_w is the water surface area.

3.3 Line of sight assumption

We assume the GPS noise, the tension cell sensor noise, and the dynamic tension independently affect the tension-distance mapping, and are modeled as Gaussian white noise. Given the all assumptions and discussion, we have a line-of-sight (LOS) assumption.

Assumption 2. (LOS). The tension-range mapping is simplified according to Assumption 1 and (9). The LOS assumption can be expressed as

$$X_{ij} = X_{ij}^0 + v_{Xij} \text{ and } X_i = X_i^0 + v_{Xi}, \quad (11)$$

where $X_{ij} = f_i^{-1}(T_{ij})$ and $X_i = f_i^{-1}(T_i)$ are the distances resulting from noisy measurements through the range mapping $f_i^{-1}(\cdot)$, where $v_{Xij} \sim N(0, \sigma_{d_{ij}}^2)$ and $v_{Xi} \sim N(0, \sigma_{d_i}^2)$, are zero-mean Gaussian white noise processes due to combination of tension cell sensor noise, dynamic tension, and GPS sensor noise. The variances of the distance mapping are

$$\sigma_{d_i}^2 = \sigma_{X_i}^2 = \frac{\sigma_{Tn_i}^2 + \sigma_{Td}^2}{k_i^2} + \sigma_{GPS}^2 \text{ and } \sigma_{d_{ij}}^2 = \sigma_{X_{ij}}^2 = \frac{\sigma_{Tn_i}^2}{k_{ij}^2}, \quad (12)$$

where σ_{Tn} and σ_{Td} denote the variances of the tension measurement caused by the sensor noise and the dynamic tension, σ_{GPS} is the variance of the GPS noise, and k_i and k_{ij} are treated as generalized stiffnesses. We consider them as constants, that is, $k_i = \frac{\partial T_{ij}}{\partial X_{ij}} \simeq$ constant.

The influence of k_i has been verified in Ren et al. (2015). The σ_{GPS}^2 in $\sigma_{d_{ij}}^2$ are neglected, since the observer will efficiently filter this noise.

Remark 1. Actually, the tension variance is no longer in a form of Gaussian white noise when considering the horizontal motion perpendicular to the cable's seafloor projection. In a static perspective, the variance in X is a nonlinear term, i.e., $\sqrt{(x-x_a)^2+(y-y_a)^2} - X_0$, when the vessel has a 3D motion. However, simulation results have shown that such influence is negligible (Ren and Skjetne, 2016).

3.4 Influence of the fairleads

Previous works always assume that all the mooring lines are connected at the COT. However, the fact is that they are connected at the fairleads, and the influence from the fairleads should not be disregarded. Assuming the friction between the turret and the vessel is negligible, the turret will rotate by the torque from the horizontal components of the mooring forces. Additionally, the magnitude of the turret radius is much smaller than the lengths of the mooring lines. The arrangement is illustrated in Fig. 3. Since the angle $\Delta\psi_t^i$ is small, we assume that the COT is located along the extension of the line from the anchor to the corresponding fairlead, with a distance r_t from the fairlead. The mathematical expression is given by

$$d_{ij} = f_i^{-1}(T_{ij}^0) + r_t + v_{Xij} \text{ and } d_i = f_i^{-1}(T_i^0) + r_t + v_{Xi}, \quad (13)$$

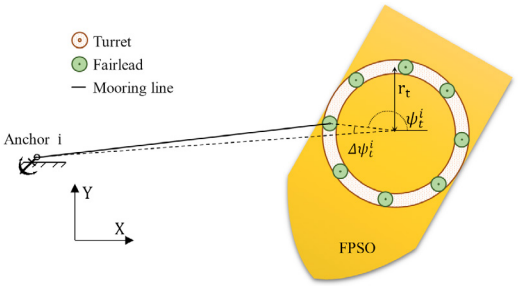

Fig. 3. The fairlead arrangement.

where d_{ij} is the distance between the i^{th} anchor and the j^{th} "virtual vessel's COT", d_i is the distance between the i^{th} anchor and the real-time COT.

Here we define two vectors, $\boldsymbol{d}_I \in \mathbb{R}^M$ and $\boldsymbol{d}_{IJ} \in \mathbb{R}^{MN}$, which contain all d_{ij} and d_i respectively. They are

$$\boldsymbol{d}_I = [d_1, d_2, \cdots, d_M]^\top, \quad (14a)$$

$$\boldsymbol{d}_{IJ} = [d_{11}, d_{12} \cdots d_{1N}, \cdots, d_{M1}, d_{M2} \cdots d_{MN}]^\top. \quad (14b)$$

4. SENSOR NETWORK CONSTRUCTION

Based on the collaborative localization method, three (or four) is the minimum number of the landmarks to locate another unknown node in a 2D (or 3D) coordinate (Shang et al., 2004). We know the position of the COT from the vessel GPS signals, but not of the anchors. Therefore, the anchors, in this case, are the uncertain nodes, while the turret is a landmark. We therefore construct a sensor network with N virtual vessels, based on previously collected and stored data, as shown in Fig. 4.

Assuming the mooring equilibrium position in a given sea state is uniformly determined by the environmental parameters such as the magnitudes and directions of the second-order wave loads, current, and wind loads. We collect and store the position data from the observers and the tension measurements when the vessel is positioning stably at different equilibrium positions. Since the data from the observer is already filtered with respected to noise and WF motion, we can directly read the data at the next time instant in the EKF update process. When recalling all the previous data, we have a group of N landmarks, which are labeled as TP_j in Fig. 4. Additionally, we have information on the best initial estimation of the anchor positions.

The objective of this paper is then to locate the vessel COT and the unknown anchors simultaneously. Then the new sensor network has N anchor nodes and $M+1$ uncertain nodes. The problem is solvable in the sense of a sensor network.

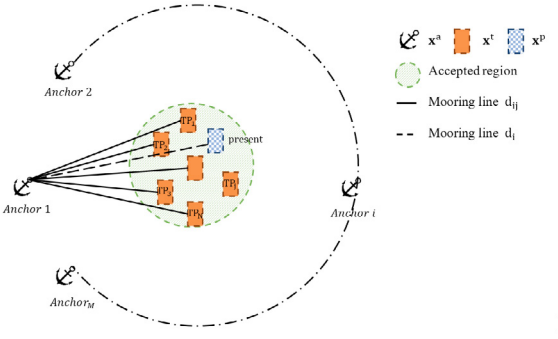

Fig. 4. Sensor network construction.

4.1 Problem statement

For the sake of simplification, we disregard the water depth and hereafter refer to t his as a 2D sensor network. The real-time position of the turret is $\boldsymbol{p}^p = [x^p, y^p]^\top$ and $\boldsymbol{\eta} = [\boldsymbol{p}^{p\top}, \psi]^\top$. The position of the i^{th} anchor is defined as $\boldsymbol{p}_i^a = [x_i^a, y_i^a]^\top$, $i = 1, \cdots, M$. The position of the j^{th} turret is defined as $\boldsymbol{p}_j^t = [x_j^t, y_j^t]^\top$, $j = 1, \cdots, N$.

Define two vectors containing all the anchor position $\boldsymbol{p}^a \in \mathbb{R}^{2M}$ and turret positions of all "virtual vessels" $\boldsymbol{p}^t \in \mathbb{R}^{2N}$ as $\boldsymbol{p}^a = \left[\boldsymbol{p}_1^{a\top} \cdots \boldsymbol{p}_M^{a\top}\right]^\top$ and $\boldsymbol{p}^t = \left[\boldsymbol{p}_1^{t\top} \cdots \boldsymbol{p}_N^{t\top}\right]^\top$. In this paper, the current influence on the tension variance is disregarded; hence, Assumption 2 is satisfied, and (13) is applied to the range measurement. The current load influence is more dominant in deep water. However, it will only introduce a bounded, small bias to the measurements, due to the high generalized stiffness k_i in (12), and is also neglected in this paper.

The problem is to estimate $\boldsymbol{p}^p$ and $\boldsymbol{p}^a$ based on $\boldsymbol{p}^t$, $\boldsymbol{d}_I$, and $\boldsymbol{d}_{IJ}$. We assume the anchors have fixed, but uncertain positions during the localization. Additionally, there is no information exchange between the anchors. The only external information is the best estimated anchor positions during installation and manual observation. Since the TAPM is always running around the equilibrium position, which is determined by the environmental loads, the stiffness k_i only depends on the cable and it is vessel-independent. In this case, k_i is in the level of 10^5.

5. THE EKF-BASED SOLUTION

Consider a system given by

$$\dot{\boldsymbol{x}} = \boldsymbol{f}(\boldsymbol{x}) + \boldsymbol{B}\boldsymbol{u} + \boldsymbol{E}\boldsymbol{w}, \tag{15a}$$
$$\boldsymbol{y} = \boldsymbol{h}(\boldsymbol{x}) + \boldsymbol{v}. \tag{15b}$$

The EKF algorithm is summarized in Table 1, where $\boldsymbol{K}(k)$ is the Kalman gain matrix, $\hat{\boldsymbol{P}}(k)$ represents the error covariance matrix, $\boldsymbol{Q} = \boldsymbol{Q}^\top$ and $\boldsymbol{R} = \boldsymbol{R}^\top$ are covariance matrices, $\boldsymbol{f}_k(\hat{\boldsymbol{x}}(k), \boldsymbol{u}_k) = \hat{\boldsymbol{x}}(k) + T[\boldsymbol{f}\hat{\boldsymbol{x}}(k) + \boldsymbol{B}\boldsymbol{u}(k)]$, $\boldsymbol{\Phi}(k) = \boldsymbol{I} + T\frac{\partial \boldsymbol{f}_k(\boldsymbol{x}(k), \boldsymbol{u}(k))}{\partial \boldsymbol{x}(k)}\big|_{\boldsymbol{x}(k)=\hat{\boldsymbol{x}}(k)}$, and $\boldsymbol{\Gamma}(k) = T\boldsymbol{E}(k)$, $\boldsymbol{H}(k) = \frac{\partial \boldsymbol{h}}{\partial \boldsymbol{x}}\big|_{\boldsymbol{x}=\bar{\boldsymbol{x}}(k)}$.

Table 1. Extended Kalman filter.

Design matrices	$\boldsymbol{Q} = \boldsymbol{Q}^\top > 0, \boldsymbol{R} = \boldsymbol{R}^\top$
Initial conditions	$\bar{\boldsymbol{x}}(0) = \boldsymbol{x}_0$
Kalman gain matrix	$\boldsymbol{K}(k) = \bar{\boldsymbol{P}}\boldsymbol{H}^\top(k)[\boldsymbol{H}(k)\bar{\boldsymbol{P}}(k)\boldsymbol{H}^\top(k) + \boldsymbol{R}(k)]^{-1}$
State estimate update	$\hat{\boldsymbol{x}}(k) = \bar{\boldsymbol{x}}(k) + \boldsymbol{K}(k)[\boldsymbol{y}(k) - \boldsymbol{g}(\bar{\boldsymbol{x}}(k))]$
Error covariance update	$\hat{\boldsymbol{P}}(k) = [\boldsymbol{I} - \boldsymbol{K}(k)\boldsymbol{H}(k)]\bar{\boldsymbol{P}}(k)[\boldsymbol{I} - \boldsymbol{K}(k)\boldsymbol{H}(k)]^\top + \boldsymbol{K}(k)\boldsymbol{R}(k)\boldsymbol{K}^\top(k)$
State estimate prop.	$\bar{\boldsymbol{x}}(k+1) = \boldsymbol{f}_k(\hat{\boldsymbol{x}}(k), \boldsymbol{u}_k)$
Error estimate prop.	$\bar{\boldsymbol{P}}(k+1) = \boldsymbol{\Phi}(k)\hat{\boldsymbol{P}}(k)\boldsymbol{\Phi}^\top(k) + \boldsymbol{\Gamma}(k)\boldsymbol{Q}(k)\boldsymbol{\Gamma}^\top(k)$

To simplify the representation, we employ the range measurements directly after the tension mapping, i.e., $\boldsymbol{d}_I$ and $\boldsymbol{d}_{IJ}$. The anchors have fixed positions, but a noise is needed to balance the distance between the estimated and the real positions. This is similar to (1b), which is applied to simulate the slowly-varying loads. The discrete form is given by $\boldsymbol{p}_i^a(k+1) = \boldsymbol{p}_i^a(k) + \boldsymbol{w}_{ai}$. The continuous form is given by $\dot{\boldsymbol{p}}^a = \boldsymbol{E}_a\boldsymbol{\omega}_a$.

The EKF is based on the overall nonlinear model

$$\boldsymbol{f}(\boldsymbol{x}) = \begin{bmatrix} \boldsymbol{A}_w\boldsymbol{\xi} \\ \boldsymbol{R}(\psi)\boldsymbol{\nu} \\ -\boldsymbol{T}_b^{-1}\boldsymbol{b} \\ \boldsymbol{M}^{-1}[-\boldsymbol{D}\boldsymbol{\nu} + \boldsymbol{R}(\psi)^\top\boldsymbol{b} - \boldsymbol{R}^\top(\psi)\boldsymbol{G}\boldsymbol{\eta} + \boldsymbol{\tau}_c] \\ \boldsymbol{0}_{2M\times 1} \\ \boldsymbol{0}_{2N\times 1} \end{bmatrix},$$

$$\boldsymbol{B} = \begin{bmatrix} \boldsymbol{0}_{6\times 3} \\ \boldsymbol{0}_{3\times 3} \\ \boldsymbol{0}_{3\times 3} \\ \boldsymbol{M}^{-1} \\ \boldsymbol{0}_{2M\times 3} \\ \boldsymbol{0}_{2N\times 3} \end{bmatrix}, \quad \boldsymbol{E} = \begin{bmatrix} \boldsymbol{E}_w & \boldsymbol{0}_{3\times 3} & \boldsymbol{0}_{6\times 2M} \\ \boldsymbol{0}_{3\times 3} & \boldsymbol{0}_{3\times 3} & \boldsymbol{0}_{3\times 2M} \\ \boldsymbol{0}_{3\times 3} & \boldsymbol{E}_b & \boldsymbol{0}_{3\times 2M} \\ \boldsymbol{0}_{3\times 3} & \boldsymbol{0}_{3\times 3} & \boldsymbol{0}_{3\times 2M} \\ \boldsymbol{0}_{2M\times 3} & \boldsymbol{0}_{2M\times 3} & \boldsymbol{E}_a \\ \boldsymbol{0}_{2N\times 3} & \boldsymbol{0}_{2N\times 3} & \boldsymbol{0}_{2N\times 2M} \end{bmatrix},$$

$$\boldsymbol{h}(\boldsymbol{x}) = \begin{bmatrix} \psi + \xi_6 \\ \boldsymbol{p}^t \\ \boldsymbol{G}_I(\boldsymbol{p}^a, \boldsymbol{\eta}) \\ \boldsymbol{G}_{IJ}(\boldsymbol{p}^a, \boldsymbol{p}^t) \end{bmatrix},$$

where the state vector is $\boldsymbol{x} = [\boldsymbol{\xi}^\top, \boldsymbol{\eta}^\top, \boldsymbol{b}^\top, \boldsymbol{\nu}^\top, \boldsymbol{p}^{a\top}, \boldsymbol{p}^{t\top}]^\top$, $\boldsymbol{\eta} = [\boldsymbol{p}^{p\top}, \psi]^\top$, the measurement vector is $\boldsymbol{y} = [\psi + \xi_6, \boldsymbol{p}^{t\top}, \boldsymbol{d}_I^\top, \boldsymbol{d}_{IJ}^\top]^\top$, and $\boldsymbol{w} = [w_w^\top, w_b^\top, w_a^\top]^\top$. The tuning matrices are $\boldsymbol{Q} \in \mathbb{R}^{(6+2M)\times(6+2M)}$ and $\boldsymbol{R} \in \mathbb{R}^{(1+2N+M+MN)\times(1+2N+M+MN)}$. The distance mapping functions are given by $\boldsymbol{d}_I = \boldsymbol{G}_I(\boldsymbol{p}^a, \boldsymbol{p}^p + [\xi_4, \xi_5]^\top)$ and $\boldsymbol{d}_{IJ} = \boldsymbol{G}_{IJ}(\boldsymbol{p}^a, \boldsymbol{p}^t)$, where the estimated distances are given by

$$d_i = g_i(\boldsymbol{p}_i^a, \boldsymbol{p}^p + [\xi_4, \xi_5]^\top) = \sqrt{(x_i^a - x^p - \xi_4)^2 + (y_i^a - y^p - \xi_5)^2},$$
$$d_{ij} = g_{ij}(x_i^a, x_j^t) = \sqrt{(x_i^a - x_j^t)^2 + (y_i^a - y_j^t)^2}.$$

The Jacobian matrix is given by

$$\boldsymbol{H} = \frac{\partial \boldsymbol{h}}{\partial \boldsymbol{x}} = \begin{bmatrix} \frac{\partial \psi}{\partial \boldsymbol{\xi}} & \frac{\partial \psi}{\partial \boldsymbol{\eta}} & \boldsymbol{0}_{1\times 3} & \boldsymbol{0}_{1\times 3} & \boldsymbol{0}_{1\times 2M} & \boldsymbol{0}_{2N\times 2N} \\ \boldsymbol{0}_{2N\times 6} & \boldsymbol{0}_{2N\times 3} & \boldsymbol{0}_{2N\times 3} & \boldsymbol{0}_{2N\times 3} & \boldsymbol{0}_{2N\times 2M} & \boldsymbol{I}_{2N\times 2N} \\ \frac{\partial \boldsymbol{d}_I}{\partial \boldsymbol{\xi}} & \frac{\partial \boldsymbol{d}_I}{\partial \boldsymbol{\eta}} & \boldsymbol{0}_{M\times 3} & \boldsymbol{0}_{M\times 3} & \frac{\partial \boldsymbol{d}_I}{\partial \boldsymbol{p}^a} & \boldsymbol{0}_{M\times 2N} \\ \boldsymbol{0}_{MN\times 6} & \boldsymbol{0}_{MN\times 3} & \boldsymbol{0}_{MN\times 3} & \boldsymbol{0}_{MN\times 3} & \frac{\partial \boldsymbol{d}_{IJ}}{\partial \boldsymbol{p}^a} & \frac{\partial \boldsymbol{d}_{IJ}}{\partial \boldsymbol{p}^t} \end{bmatrix} \tag{16}$$

where

$$\frac{\partial \psi}{\partial \boldsymbol{\xi}} = [0\ 0\ 0\ 0\ 0\ 1], \ \frac{\partial \psi}{\partial \boldsymbol{\eta}} = [0\ 0\ 1],$$
$$\frac{\partial \boldsymbol{d}_I}{\partial \boldsymbol{\xi}} = [\boldsymbol{0}_{M\times 3},\ \boldsymbol{A}_1\boldsymbol{A}_2\boldsymbol{A}_3,\ \boldsymbol{0}_{M\times 1}], \ \frac{\partial \boldsymbol{d}_I}{\partial \boldsymbol{\eta}} = [\boldsymbol{A}_1\boldsymbol{A}_2\boldsymbol{A}_3,\ \boldsymbol{0}_{M\times 1}],$$
$$\boldsymbol{A}_1 = diag\{\frac{1}{d_1}, \frac{1}{d_2}, \cdots, \frac{1}{d_M}\}, \ \boldsymbol{A}_2 = [\boldsymbol{1}_{M\times 2}, -\boldsymbol{I}_{M\times M}],$$
$$\boldsymbol{A}_3 = [\boldsymbol{p}^p, [\xi_4, \xi_5]^\top, \boldsymbol{p}_1^a, \boldsymbol{p}_2^a, \cdots, \boldsymbol{p}_M^a]^\top,$$
$$\frac{\partial \boldsymbol{d}_I}{\partial \boldsymbol{p}^a} = \begin{bmatrix} \boldsymbol{\chi}_1 & \boldsymbol{0}_{2\times 1} & \cdots & \boldsymbol{0}_{2\times 1} \\ \boldsymbol{0}_{2\times 1} & \boldsymbol{\chi}_2 & \cdots & \boldsymbol{0}_{2\times 1} \\ \vdots & \vdots & \ddots & \vdots \\ \boldsymbol{0}_{2\times 1} & \boldsymbol{0}_{2\times 1} & \cdots & \boldsymbol{\chi}_M \end{bmatrix}, \ \boldsymbol{\chi}_i = \begin{bmatrix} \frac{x^p + \xi_4 - x_i^a}{d_1} & \frac{y^p + \xi_5 - y_i^a}{d_1} \end{bmatrix},$$
$$\frac{\partial \boldsymbol{d}_{IJ}}{\partial \boldsymbol{p}^a} = \begin{bmatrix} \boldsymbol{\varsigma}_1 & \boldsymbol{0}_{N\times 2} & \cdots & \boldsymbol{0}_{N\times 2} \\ \boldsymbol{0}_{N\times 2} & \boldsymbol{\varsigma}_2 & \cdots & \boldsymbol{0}_{N\times 2} \\ \vdots & \vdots & \ddots & \vdots \\ \boldsymbol{0}_{N\times 2} & \boldsymbol{0}_{N\times 2} & \cdots & \boldsymbol{\varsigma}_M \end{bmatrix}, \boldsymbol{\varsigma}_i = \begin{bmatrix} \frac{x_i^a - x_1^t}{d_{i1}} & \frac{y_i^a - y_1^t}{d_{i1}} \\ \frac{x_i^a - x_2^t}{d_{i2}} & \frac{y_i^a - y_2^t}{d_{i2}} \\ \vdots & \vdots \\ \frac{x_i^a - x_N^t}{d_{iN}} & \frac{y_i^a - y_N^t}{d_{iN}} \end{bmatrix},$$
$$\frac{\partial \boldsymbol{d}_{IJ}}{\partial \boldsymbol{p}^t} = \begin{bmatrix} \boldsymbol{\vartheta}_1^\top & \boldsymbol{\vartheta}_2^\top & \cdots & \boldsymbol{\vartheta}_M^\top \end{bmatrix}^\top,$$
$$\boldsymbol{\vartheta}_i = \begin{bmatrix} \boldsymbol{\vartheta}_{i1} & & & \\ & \boldsymbol{\vartheta}_{i2} & & \\ & & \ddots & \\ & & & \boldsymbol{\vartheta}_{iN} \end{bmatrix}, \ \boldsymbol{\vartheta}_{ij} = \begin{bmatrix} \frac{x_j^t - x_i^a}{d_{ij}} & \frac{y_j^t - y_i^a}{d_{ij}} \end{bmatrix}.$$

Remark: We notice that the matrix $\frac{\partial \boldsymbol{d}_{IJ}}{\partial \boldsymbol{p}^a}$ and $\frac{\partial \boldsymbol{d}_{IJ}}{\partial \boldsymbol{p}^t}$ are made up of M blocks. To write it in this form has an advantage that every

block is related to one anchor. In other words, we can choose the relevant anchors to construct the matrices.

In practice, we may have more available information than the model we have introduced. For instance, when the anchor positions are all well-known, we may only estimate the moored vessel based on the tension measurements. Furthermore, note that the only interesting information may be the location of the anchor when the vessel has lost it. These scenarios will be presented in further work.

6. NUMERICAL SIMULATION

6.1 Overview

The simulations are conducted in Simulink® with the Marine System Simulator (MSS) toolbox (MSS, 2010). An FPSO is moored by eight mooring lines with a turret $r_t = 20\ m$. The parameters of the mooring lines are tabulated in Table 2. The time step is 0.02 s. Due to the page limit, the observability analysis and more detailed simulation results with biases will be presented in a further publication.

Table 2. Mooring line dimensions.

Principle Dimension	Values
Dens. of ambient water $\rho_w(kg/m^3)$	1025
Dens. of ambient water $\rho_0(kg/m)$	275
Length of the cable $L_m(m)$	2250
Elastic modulus $E(Pa)$	4.5757×10^{10}
Cable cross section area $A_m(m^2)$	0.005
Cable diameter $d_m(m)$	0.08
Max strain ε	0.005
Normal drag coefficient C_{DN}	0.3
Tangential drag coefficient C_{DT}	1.0
Added mass coefficient C_{MN}	1.5

To collect the data for the virtual vessels, a group of simulations in various environments are conducted. All the environmental parameters are generated randomly, including the wind speed and direction, the significant wave height and its main direction, the current speed and direction, and the initial estimated anchor positions. The current direction is randomly set in a $\pm 35\ deg$ region from the main wave direction. The controller only controls the heading. Data are only collected after the vessel has been stabilized at a new equilibrium position given by the different environmental parameters.

Then we have a set of virtual vessels running in different environments at a group of equilibrium positions. We assume there exist 10 virtual vessels. The initial estimation of the anchor positions are concluded in Table 4. Furthermore, a group of simulations are conducted to evaluate the effects of the number of virtual vessel N to the localization performance. Every simulation in the group shares the same stored data and accesses the measurement at the same time instant. Specifically, we select $N = 4$, 7, and 10. The real position and the initial estimates are tabulated in Table 4.

To verify the robustness of this algorithm, we assume large variance in the tension cells, i.e., $\sigma_{T_i}^2 = 10^8$, which is much larger than a practical situation. Hence, the distance from the mapping suffers greatly from noise. Additionally, all the tension cells are independent.

6.2 Simulation results and discussion

The simulations end at $100\,s$. Running time with $4/7/10$ virtual vessels are $67.2/67.2/154.5$ seconds, respectively. We notice, the computational time depends on the number of virtual vessels. The simulation results are shown in Fig. 5 and Fig. 6.

Table 3. Virtual vessel equilibrium positions.

Index $[j]$	Equilibrium positions $[x_j^t, y_j^t]^\top(m)$	Wind $v_{wind}(m/s)$ $\beta_{wind}(deg)$	Wave $H_s(m)$ $\beta_{wave}(deg)$	Current $v_{cur}(m/s)$ $\beta_{cur}(deg)$
1	$[-11.0, 18.9]^\top$	4.0, 147.3	2.53, 27.5	0.17, 67.2
2	$[-1.9, 3.9]^\top$	1.3, 34.8	4.4, 150	0.002, 118.4
3	$[32.8, 29.1]^\top$	4.2, 80.2	1.9, 34.6	0.79, 24.1
4	$[57.6, -25.4]^\top$	5.1, 2.3	4.6, 115.1	0.51, 98.0
5	$[21.7, -12.8]^\top$	0.13, 55.6	3.0, 120.55	0.21, 90.6
6	$[-2.3, 5.4]^\top$	6.7, 157.6	4.9, 139.1	0.10, 174.7
7	$[20.6, 9.0]^\top$	6.42, 150.4	6.18, 68.4	0.16, 52.4
8	$[51.7, 14.1]^\top$	5.58, 60.0	4.44, 79.5	0.41, 100.5
9	$[53.4, 4.9]]^\top$	3.7, 158.6	6.9, 87.0	00.41, 78.9
10	$[1.6, -1.6]^\top$	0.7, 86.4	5.75, 109.5	0.05, 100.4

Table 4. Anchor positions and initial estimations.

Index $[i]$	Position of the anchors $[x_i^a, y_i^a, z_i^a]^\top(m)$	Initial estimation $[\bar{x}_i^a(0), \bar{y}_i^a(0), \bar{z}_i^a(0)]^\top(m)$
1	$[2030, 0, -1000]^\top$	$[1931.5, 148.2, -1000]^\top$
2	$[1385.9, 1385.9, -1000]^\top$	$[1734.6, 1520.8, -1000]^\top$
3	$[0, 2030, -1000]^\top$	$[-101.3, 2234.2, -1000]^\top$
4	$[-1385.9, 1385.9, -1000]^\top$	$[-1601.6, 1568.6, -1000]^\top$
5	$[-2030, 0, -1000]^\top$	$[-2176.4, -262.7, -1000]^\top$
6	$[-1385.9, -1385.9, -1000]^\top$	$[-1621.5, -1298.5, -1000]^\top$
7	$[0, -2030, -1000]^\top$	$[125.3, -2359.0, -1000]^\top$
8	$[1385.9, -1385.9, -1000]^\top$	$[1355.8, -1596.0, -1000]^\top$

The top tension depends on the position of the node with index $k = n - 1$. However, the initial position of $\boldsymbol{r}_{n-1}^i$ is not perfectly initialized. Hence, the tension measurements oscillate and reach sudden maxima at $t = 0\ s$.

The red, blue, and black lines are the values estimated through the tension estimation. The green curve is the noisy GPS measurement. We can find that the anchor positions and the real-time LF motion are well estimated. Additionally, the wave-induced motion can be eliminated well. The performance mainly depends on the parametric tuning and variances of the noise in the tension measurements.

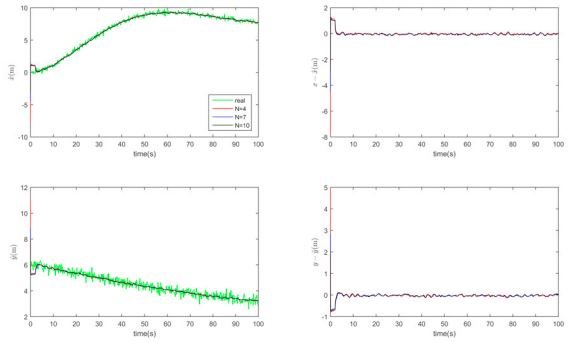

Fig. 5. Real-time estimation of the vessel position.

The anchor position $\boldsymbol{p}^t$ quickly converges and stays bounded around the real positions. The convergence speed largely depends on the choice of the matrices, such as $\boldsymbol{E}_a$, $\boldsymbol{Q}$, and $\boldsymbol{R}$. The simulation results show the estimation of the anchor positions is slower than the real-time localization of the moored vessel. We notice that there exists an oscillation between the estimated and real position, but it still locates the anchors well. The performance improves when the variance of the tension cells reduces. The configuration with $N = 10$ only slightly improves the results compared to the configuration with $N = 4$.

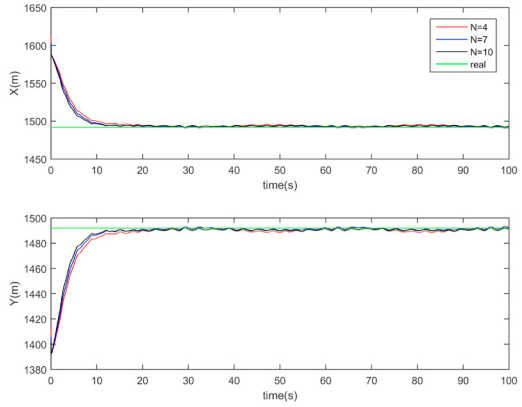

(a) Anchor 2

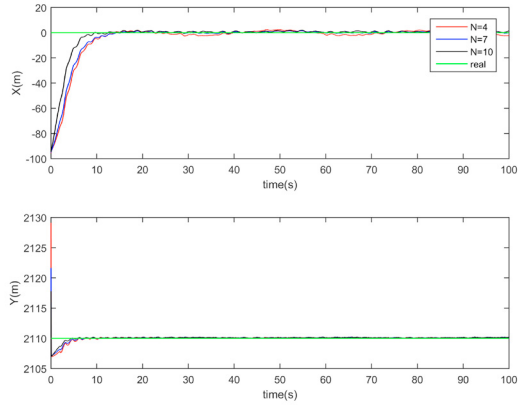

(b) Anchor 3

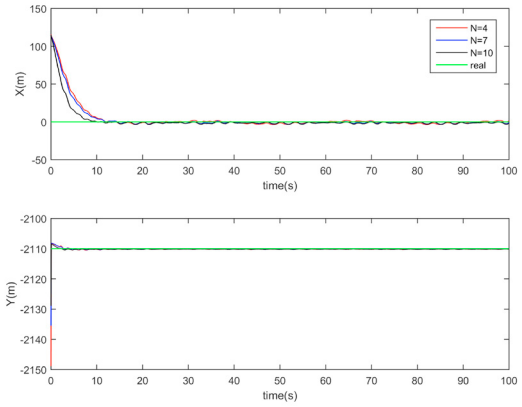

(c) Anchor 7

Fig. 6. Real time estimation of the anchor positions.

7. CONCLUSION AND FUTURE WORKS

This paper illustrates the process to apply the map aided localization algorithm to a TAPM system to locate the vessel as well as the uncertain anchors. A sensor network scheme is built with the previously stored data. The influence of the turret is discussed to provide a more realistic solution. Range measurement noise is analyzed. EKF is employed to asymptotically estimate the uncertain nodes. Numerical simulations was conducted to verify it. Future emphasis will be placed on the non-line-of-sight tension measurements, including the current influence, model uncertainty, and sensor biases.

REFERENCES

Aamo, O.M. (1999). *Adding mooring systems to the ABB Integrated Vessel Simulator Implementation*. Department of Engineering Cybernetics, NTNU, Trondheim, Norway.

Aamo, O.M. and Fossen, T.I. (1999). Controlling line tension in thruster assisted mooring systems. In *Control Applications, 1999. Proceedings of the 1999 IEEE International Conference on*, volume 2, 1104–1109. IEEE.

Aamo, O. and Fossen, T. (2001). Finite element modelling of moored vessels. *Mathematical and Computer Modelling of Dynamical Systems*, 7(1), 47–75.

Durrant-Whyte, H. and Bailey, T. (2006). Simultaneous localization and mapping: part i. *Robotics & Automation Magazine, IEEE*, 13(2), 99–110.

Fossen, T.I. (2011). *Handbook of marine craft hydrodynamics and motion control*. John Wiley & Sons.

Gard News (2011). Loss of anchors and chain. URL `http://www.gard.no/ikbViewer/web/updates/content/11831736/loss-of-anchors-and-chain`.

Gustafsson, F. (2010). *Statistical sensor fusion*. Studentlitteratur, Lund, Sweden.

Ji, S., Choi, M., and Kim, Y. (2015). A study on position mooring system design for the vessel moored by mooring lines. *Mechatronics, IEEE/ASME Transactions on*, PP(99), 1–8.

May, P., Sanderson, D., Sharp, J., and Stacey, A. (2008). Structural integrity monitoring: Review and appraisal of current technologies for offshore applications. In *ASME 2008 27th International Conference on Offshore Mechanics and Arctic Engineering*, 247–263. American Society of Mechanical Engineers.

MSS. Marine Systems Simulator (2010). Viewed 30.10.2014. URL `http://www.marinecontrol.org`.

Naddafzadeh-Shirazi, G., Shenouda, M.B., and Lampe, L. (2014). Second order cone programming for sensor network localization with anchor position uncertainty. *Wireless Communications, IEEE Transactions on*, 13(2), 749–763.

Nguyen, D.H., Nguyen, D.T., Quek, S.T., and Sørensen, A.J. (2011). Position-moored drilling vessel in level ice by control of riser end angles. *Cold Regions Science and Technology*, 66(2-3), 65–74.

Oxford Advanced Learner's Dictionary (n.d.). Viewed 28.04.2015. URL `http://www.oxforddictionaries.com/definition/english/anchor`.

Ratcovich, M. (2008). The nairobi international convention on the removal of wrecks in light of existing marine liability regimes.

Ren, Z. and Skjetne, R. (2016). An on-site current profile estimation algorithm for a moored floating structure. *IFAC-PapersOnLine*.

Ren, Z., Skjetne, R., and Kjerstad, Ø.K. (2015). A tension-based position estimation approach for moored marine vessels. *IFAC-PapersOnLine*, 48(16), 248 – 253.

Shang, Y., Rumi, W., Zhang, Y., and Fromherz, M. (2004). Localization from connectivity in sensor networks. *Parallel and Distributed Systems, IEEE Transactions on*, 15(11), 961–974.

Skjetne, R., Imsland, L., and Løset, S. (2014). The arctic DP research project: Effective stationkeeping in ice. 191–210.

Tseng, P. (2007). Second-order cone programming relaxation of sensor network localization. *SIAM Journal on Optimization*, 18(1), 156–185.

Zekavat, R. and Buehrer, R.M. (2011). Collaborative position location. In R.M. Buehrer and T. Jia (eds.), *Handbook of position location: Theory, practice and advances*, chapter 12, 755–810. John Wiley & Sons.